



Atomic Gas Dominates the Baryonic Mass of Star-forming Galaxies at $z \approx 1.3$

Aditya Chowdhury , Nissim Kanekar , and Jayaram N. Chengalur

National Centre for Radio Astrophysics, Tata Institute of Fundamental Research, Pune, India; nkanekar@ncra.tifr.res.in

Received 2022 June 1; revised 2022 July 12; accepted 2022 July 15; published 2022 August 10

Abstract

We present a comparison between the average atomic gas mass, $\langle M_{\text{Atom}} \rangle$ (including hydrogen and helium), the average molecular gas mass, $\langle M_{\text{Mol}} \rangle$, and the average stellar mass, $\langle M_{\star} \rangle$, of a sample of star-forming galaxies at $z \approx 0.75\text{--}1.45$ to probe the baryonic composition of galaxies in and during the epoch of peak star formation activity in the universe. The $\langle M_{\text{Atom}} \rangle$ values of star-forming galaxies in two stellar-mass-matched samples at $z = 0.74\text{--}1.25$ and $z = 1.25\text{--}1.45$ were derived by stacking their HI 21 cm signals in the GMRT-CAT_{z1} survey. We find that the baryonic composition of star-forming galaxies at $z \gtrsim 1$ is dramatically different from that at $z \approx 0$. For star-forming galaxies with $\langle M_{\star} \rangle \approx 10^{10} M_{\odot}$, the contribution of stars to the total baryonic mass, M_{Baryon} , is $\approx 61\%$ at $z \approx 0$, but only $\approx 16\%$ at $z \approx 1.3$, while molecular gas constitutes $\approx 6\%$ of the baryonic mass at $z \approx 0$, and $\approx 14\%$ at $z \approx 1.3$. Remarkably, we find that atomic gas makes up $\approx 70\%$ of M_{Baryon} in star-forming galaxies at $z \approx 1.3$. We find that the ratio $\langle M_{\text{Atom}} \rangle / \langle M_{\star} \rangle$ is higher at both $z \approx 1.3$ and at $z \approx 1.0$ than in the local universe, with $\langle M_{\text{Atom}} \rangle / \langle M_{\star} \rangle \approx 1.4$ at $z \approx 1.0$ and ≈ 4.4 at $z \approx 1.3$, compared to its value of ≈ 0.5 today. Further, we find that the ratio $\langle M_{\text{Atom}} \rangle / \langle M_{\text{Mol}} \rangle$ in star-forming galaxies with $\langle M_{\star} \rangle \approx 10^{10} M_{\odot}$ is ≈ 2.3 at $z \approx 1.0$ and ≈ 5.0 at $z \approx 1.3$. Overall, we find that atomic gas is the dominant component of the baryonic mass of star-forming galaxies at $z \approx 1.3$, during the epoch of peak star formation activity in the universe.

Unified Astronomy Thesaurus concepts: Galaxies (573); High-redshift galaxies (734); Neutral hydrogen clouds (1099)

1. Introduction

Neutral atomic hydrogen (HI) and molecular hydrogen (H_2) are the key components of the cold interstellar medium (ISM) in galaxies and are the fuel for star formation. The distribution of baryons between atomic gas, molecular gas, and stars is an important indicator of the evolutionary stage of a galaxy: At early times, most of the baryonic mass is in the atomic phase, while, for highly evolved systems (e.g., red and dead ellipticals), almost all the baryons are in the stars. The relative contributions of atomic gas, molecular gas, and stars to the total baryonic mass in galaxies and the evolution of these contributions over cosmological time are thus critical inputs to studies of galaxy evolution. In the local universe, most of the baryonic content in massive star-forming galaxies at $z \approx 0$ is in stars, while HI makes up $\approx 70\%$ – 90% of the cold gas content of most galaxies (e.g., Saintonge et al. 2017; Catinella et al. 2018).

At high redshifts, CO observations of star-forming galaxies at $z \approx 1\text{--}3$ have found evidence for large reservoirs of molecular gas, comparable in mass to their stellar masses (e.g., Daddi et al. 2010; Tacconi et al. 2013, 2018). This is very different from the situation in galaxies at $z \approx 0$, where the ratio of the molecular gas mass to the stellar mass is only $\approx 0.02\text{--}0.10$ (Saintonge et al. 2017). Indeed, the molecular gas mass of main-sequence galaxies has been observed to increase by approximately an order of magnitude from $z \approx 0$ to $z \approx 2$ (e.g., Genzel et al. 2015; Tacconi et al. 2020). The large inferred molecular gas content of high- z galaxies has been used to argue that the cold gas content of galaxies at $z \approx 1\text{--}3$ is predominantly of molecular form (e.g., Tacconi et al. 2018).

Measurements of the atomic and molecular content of high- z galaxies provide important constraints on numerical and semianalytical models of galaxy evolution (e.g., Obreschkow & Rawlings 2009; Lagos et al. 2011; Popping et al. 2014; Davé et al. 2019, 2020). Unfortunately, the weakness of the HI 21 cm line, the only tracer of the HI content of galaxies, has made it very challenging to directly measure the HI mass of galaxies at cosmological distances. Indeed, even at intermediate redshifts, there are only a handful of galaxies at $z \approx 0.2\text{--}0.4$ for which estimates of $M_{\text{Atom}}/M_{\text{Mol}}$ are available (Cybulski et al. 2016; Fernández et al. 2016; Cortese et al. 2017). As a result, it has hitherto not been possible to measure the redshift evolution of $M_{\text{Atom}}/M_{\text{Mol}}$ and directly test the hypothesis that most of the cold gas in star-forming galaxies at $z \approx 1\text{--}3$ is in the molecular phase.

Recently, the HI 21 cm stacking approach has been used to measure the average HI mass of star-forming galaxies out to $z \approx 1.3$ (Bera et al. 2019; Chowdhury et al. 2020, 2021). Chowdhury et al. (2020) used the upgraded Giant Metrewave Radio Telescope (GMRT) to measure, for the first time, the average HI mass of galaxies at $z \approx 1$ by stacking the HI 21 cm emission signals of 7653 blue star-forming galaxies at $z = 0.74\text{--}1.45$ in the DEEP2 survey fields (Newman et al. 2013). More recently, Chowdhury et al. (2022a, hereafter C22a) used the GMRT Cold-HI AT $z \approx 1$ (CAT_{z1}) survey (Chowdhury et al. 2022b; hereafter C22b), a 510 hr upgraded GMRT HI 21 cm emission survey of galaxies at $z = 0.74\text{--}1.45$, also in the DEEP2 survey fields, to measure the average HI mass of star-forming galaxies in two stellar-mass-matched subsamples at $z = 0.74\text{--}1.25$ and $z = 1.25\text{--}1.45$. C22a found that the average HI mass of main-sequence galaxies declines steeply from $z \approx 1.3$ to $z \approx 1.0$, by a factor of 3.2 ± 0.8 .

In this Letter, we combine the GMRT-CAT_{z1} measurements of the average HI mass of star-forming galaxies at $z \gtrsim 1$ with estimates of the average molecular gas mass and the average

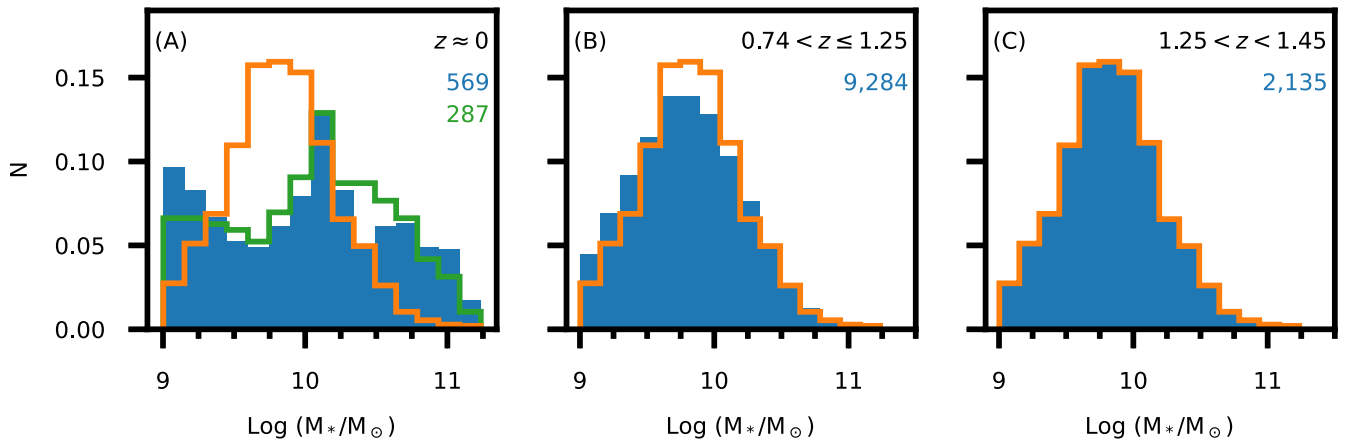


Figure 1. The stellar-mass distributions of the galaxies in the three redshift intervals. Panel (A) shows the stellar-mass distributions of the blue galaxies of the xGASS sample (blue histogram; Catinella et al. 2018) and those of the xCOLD GASS sample (green histogram; Saintonge et al. 2017). Panels (B) and (C) show the stellar-mass distributions of the GMRT-CAT z 1 subsamples at $z = 0.74$ – 1.25 and $z = 1.25$ – 1.45 (blue histograms; C22a). All average quantities reported in this work, for the three subsamples at $z \approx 0$, $z \approx 1.0$, and $z \approx 1.3$, were computed with weights such that the stellar-mass distribution of each subsample is identical to that of the subsample at $z = 1.25$ – 1.45 (the orange histogram in each panel). The number of galaxies in each subsample is listed in each panel.

stellar mass of the same galaxies to estimate, for the first time, the contribution of atomic gas, molecular gas, and stars to the baryonic mass of galaxies at $z \gtrsim 1$, nearly nine billion years ago.

Throughout this Letter, we use a flat Lambda-cold dark matter cosmology, with $\Omega_m = 0.3$, $\Omega_\Lambda = 0.7$, and $H_0 = 70 \text{ km s}^{-1} \text{ Mpc}^{-1}$. All estimates of stellar masses and SFRs assume a Chabrier initial mass function (IMF); stellar masses and SFRs from the literature that assume a Salpeter IMF were converted to a Chabrier IMF by subtracting 0.2 dex (e.g., Madau & Dickinson 2014).

2. The Cold Gas Content of Galaxies at $z \approx 1$ and in the Local Universe

2.1. Atomic Gas in Star-forming Galaxies at $z = 0.74$ – 1.45

The GMRT-CAT z 1 survey provides measurements of the average HI mass of star-forming galaxies in two stellar-mass-matched subsamples at $z = 0.74$ – 1.25 and $z = 1.25$ – 1.45 (C22a). The HI 21 cm stacking analysis used to obtain the average HI mass estimates is described in detail in C22a. We provide here a summary of the relevant information on the sample of galaxies, and the HI 21 cm stacking analysis and results, for the two redshift intervals.

The main sample of the GMRT-CAT z 1 survey contains 11,419 blue star-forming galaxies with stellar mass $M_* \geq 10^9 M_\odot$ at $z = 0.74$ – 1.45 in seven GMRT pointings on the DEEP2 survey fields (C22b). The stellar masses of the 11,419 galaxies were inferred from their rest-frame $U - B$ colors, rest-frame $B - V$ colors, and rest-frame absolute B -band magnitudes (Weiner et al. 2009); the relation was calibrated via comparisons with DEEP2 galaxies at similar redshifts in regions with K -band photometry (Weiner et al. 2009). The SFRs of the 11,419 galaxies of our sample were inferred using a calibration from Mostek et al. (2012), based on their rest-frame B -band magnitudes and the rest-frame ($U - B$) colors.¹

¹ This SFR calibration was derived by Mostek et al. (2012) for DEEP2 galaxies in the Extended Groth Strip for which SFRs were obtained by Salim et al. (2009) via spectral-energy distribution (SED) fits to the ultraviolet, optical, and near-infrared photometry. Salim et al. (2009) found the SFRs inferred from the SED fits to be consistent with the mid-infrared luminosities of the DEEP2 galaxies.

Dividing the galaxies into multiple redshift and stellar-mass bins, the average stellar masses and the average SFRs of galaxies in each bin are found to be consistent with the star-forming main sequence (Whitaker et al. 2014) at these redshifts (C22a).

The GMRT-CAT z 1 survey provides HI 21 cm subcubes for the 11,419 galaxies at a spatial resolution of 90 kpc and a velocity resolution of 90 km s^{-1} (C22b). The subcubes of each galaxy were converted from flux density (S_{HI} , in units of Jy) to luminosity density (L_{HI} , in units of Jy Mpc^2) using the relation $L_{\text{HI}} = 4\pi S_{\text{HI}} D_L^2 / (1 + z)$, where D_L is the luminosity distance of the galaxy, in Mpc. The spatial resolution of 90 kpc was chosen to ensure that the average HI 21 cm emission from the full sample of 11,419 galaxies is spatially unresolved (C22b).

The measurement of the average HI mass of galaxies in the two redshift bins was obtained by dividing the 11,419 galaxies into two redshift subsamples, with $z = 0.74$ – 1.25 (9284 galaxies) and $z = 1.25$ – 1.45 (2135 galaxies), and separately stacking the HI 21 cm subcubes of the galaxies in each subsample (C22a). The effective stellar-mass distributions of the two redshift subsamples were made identical by applying weights to the galaxies of the lower- z sample during the stacking procedure; the stellar-mass distributions of the two redshift subsamples are shown in Figure 1. The average stellar mass of the subsample at $z \approx 1.3$ is $\approx 10^{10} M_\odot$. The stacked HI 21 cm spectral cube of each subsample of galaxies was then obtained by using the above weights to take a weighted average of the HI 21 cm subcubes of the DEEP2 galaxies in each subsample. The rms noise on each of the stacked HI 21 cm spectral cubes was estimated using Monte Carlo simulations, taking into account the stellar-mass-based weights of the galaxies in each subsample (C22a). We note that the final stacked GMRT HI 21 cm spectral cubes have a spatial resolution of 90 kpc. The compact GMRT beam ensures that the measurements of the average HI mass of galaxies in the GMRT-CAT z 1 survey are not significantly affected by HI 21 cm emission from companion galaxies around the target galaxies, i.e., by source confusion (C22b).

The average HI masses of the galaxies in the two redshift subsamples were derived from their stacked HI 21 cm subcubes using the following procedure: (i) the central velocity channels of the stacked cube were averaged to obtain a stacked

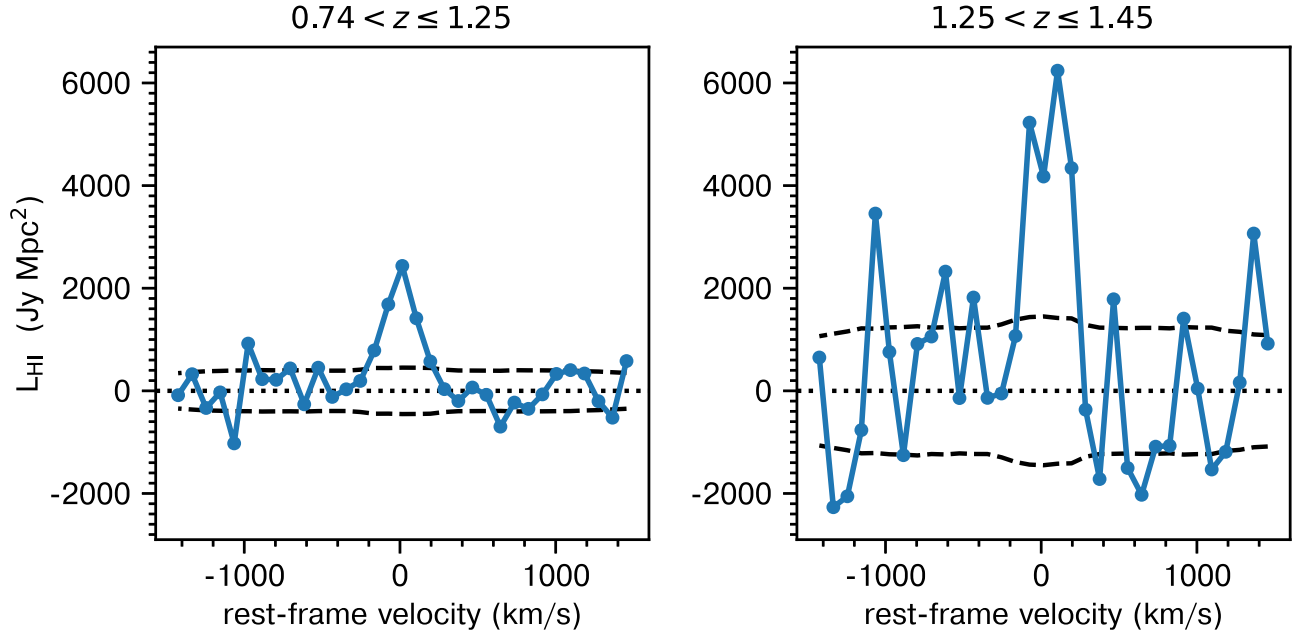


Figure 2. The stacked HI 21 cm spectra of blue star-forming galaxies at $z = 0.74$ – 1.25 (left panel) and $z = 1.25$ – 1.45 (right panel) from C22b. The stacked HI 21 cm spectrum of each panel was obtained by stacking the individual HI 21 cm spectra of the galaxies in the subsample, using weights to ensure that the stellar-mass distributions of the two subsamples are identical. The dashed curve in each panel shows the 1σ rms noise error on each 90 km s^{-1} velocity channel of the stacked HI 21 cm spectrum.

Table 1

Average Masses of the Key Baryonic Constituents of Stellar-mass-matched Samples of Blue Star-forming Galaxies at $z \approx 0$, $z \approx 1$, and $z \approx 1.3$

| | $z \approx 0$ | $z \approx 1$ | $z \approx 1.3$ |
|---|-------------------|-----------------|-----------------|
| Average stellar mass, $\langle M_* \rangle$ ($10^9 M_\odot$) | 10.3 ± 2.4 | 10.3 ± 2.4 | 10.3 ± 2.4 |
| Average atomic gas mass, $\langle M_{\text{Atom}} \rangle$ ($10^9 M_\odot$) | 5.59 ± 0.24 | 14.4 ± 2.6 | 45.7 ± 8.7 |
| Average molecular gas mass, $\langle M_{\text{Mol}} \rangle$ ($10^9 M_\odot$) | 0.974 ± 0.048 | 6.22 ± 0.78 | 9.19 ± 1.17 |
| Average baryonic mass, $\langle M_{\text{Baryon}} \rangle$ ($10^9 M_\odot$) | 16.86 ± 2.4 | 30.9 ± 3.6 | 65.3 ± 9.1 |

Note. The four rows list, for each redshift, (1) the average stellar mass, $\langle M_* \rangle$, (2) the average atomic gas mass, $\langle M_{\text{Atom}} \rangle$, including the mass contribution from helium, (3) the average molecular gas mass, $\langle M_{\text{Mol}} \rangle$, again including the mass contribution from helium, and (4) the total average baryonic mass, $\langle M_{\text{Baryon}} \rangle \equiv \langle M_* \rangle + \langle M_{\text{Atom}} \rangle + \langle M_{\text{Mol}} \rangle$. The average atomic gas masses of blue star-forming galaxies at $z \approx 1.0$ and $z \approx 1.3$ are from the GMRT-CATz1 survey (C22a), with the average molecular gas masses of the same galaxies estimated using Equation (1) (Tacconi et al. 2020). The average atomic gas and molecular gas masses of blue star-forming galaxies at $z \approx 0$ were obtained, respectively, from the xGASS and xCOLD GASS surveys (Saintonge et al. 2017; Catinella et al. 2018). The errors indicate the 1σ uncertainties in the estimates. See the text for a discussion.

HI 21 cm emission image of the subsample, (ii) the HI 21 cm spectrum at the location of the peak luminosity density in the stacked HI 21 cm emission image was extracted, (iii) contiguous central velocity channels of the stacked spectrum, with emission detected at $>1.5\sigma$ statistical significance, were integrated to measure the average velocity-integrated HI 21 cm line luminosity ($\int L_{\text{HI}} dV$, in units of $\text{Jy Mpc}^2 \text{ km s}^{-1}$) of the subsample, and (iv) the average velocity-integrated line luminosity was converted to the average HI mass of the subsample via the relation $M_{\text{HI}} = [1.86 \times 10^4 \times \int L_{\text{HI}} dV] M_\odot$.

The stacked HI 21 cm emission spectra of the 9284 galaxies at $z = 0.74$ – 1.25 and the 2135 galaxies at $z = 1.25$ – 1.45 are shown in Figure 2. For both redshift subsamples, the stacked HI 21 cm emission signal is clearly detected, at $>5.2\sigma$ statistical significance. We convert the measured average HI mass of galaxies in each subsample to an estimate of the average atomic gas mass of the subsample using the relation $\langle M_{\text{Atom}} \rangle = 1.36 \times \langle M_{\text{HI}} \rangle$, where the factor of 1.36 accounts for the mass contribution of helium. The average atomic gas masses of the galaxies in the two subsamples are listed in Table 1.

2.2. Atomic Gas in Star-forming Galaxies at $z \approx 0$

We use the extended GALEX Arcibo SDSS Survey (xGASS; Catinella et al. 2018) of nearby galaxies as a reference sample to compare the HI properties of galaxies at $z \gtrsim 1$ to those of galaxies in the local universe. xGASS is a HI 21 cm survey of a stellar-mass-selected sample of local universe galaxies with $M_* > 10^9 M_\odot$ (Catinella et al. 2018). Each galaxy in the xGASS sample was observed with the Arcibo Telescope until either a detection of the HI 21 cm emission was obtained or a 3σ upper limit of ≤ 0.1 was achieved on the ratio of the HI mass to the stellar mass. In order to carry out a fair comparison with our sample of blue star-forming galaxies at $z \approx 1$, we used only the 569 blue xGASS galaxies, with $\text{NUV} - r < 4$, as the reference sample. The stellar masses of all the xGASS galaxies are available from the Sloan Digital Sky Survey DR7 MPA-JHU catalog (Kauffmann et al. 2003; Brinchmann et al. 2004); Figure 1(A) shows the stellar-mass distribution of the 569 blue xGASS galaxies.

We measured the average HI mass of the blue xGASS galaxies, using weights such that the stellar-mass distribution of the blue xGASS sample is identical to that of our DEEP2 galaxies at $z = 1.25\text{--}1.45$. The HI 21 cm line was not detected for 16 of the 569 blue galaxies; for these 16 galaxies, we assume that the HI mass is equal to the 3σ upper limit on M_{HI} . The error on the average HI mass was estimated using bootstrap resampling with replacement. We note that we used the same stellar-mass-based weights during the bootstrap resampling procedure in order to compute the weighted-average HI mass of each randomly drawn subsample. Finally, we again converted the average HI mass of the sample to the average atomic gas mass via the relation $\langle M_{\text{Atom}} \rangle = 1.36 \times \langle M_{\text{HI}} \rangle$. Table 1 lists the average atomic gas mass of the blue xGASS galaxies at $z \approx 0$, with $\langle M_{\star} \rangle \approx 10^{10} M_{\odot}$.

2.3. Molecular Gas in Star-forming Galaxies at $z = 0.74\text{--}1.45$

The molecular gas mass of galaxies is typically estimated from tracers of molecular gas, such as the CO rotational lines, the far-infrared dust continuum, or the 1 mm dust continuum (e.g., Tacconi et al. 2020), with the different methods based on different assumptions and calibration schemes. Tacconi et al. (2020) used a compilation of molecular gas mass estimates from the literature (including the mass contribution from helium) to provide the following relation between the molecular gas depletion timescale ($t_{\text{dep,mol}} = M_{\text{Mol}}/\text{SFR}$) of galaxies and their (i) redshift, (ii) stellar mass, and (iii) offset from the star-forming main sequence at the galaxy redshift:

$$\begin{aligned} \log[t_{\text{dep,mol}}/\text{Gyr}] = & A - B \times \log[1 + z] \\ & + C \times \log[\text{sSFR}/\text{sSFR}(\text{MS}, z, M_{\star})] + D \\ & \times (\log[M_{\star}/M_{\odot}] - 10.7), \end{aligned} \quad (1)$$

where $\text{sSFR} (\equiv \text{SFR}/M_{\star})$ is the specific star formation rate, $\text{sSFR}(\text{MS}, z, M_{\star})$ is the sSFR of galaxies with stellar mass M_{\star} lying on the star-forming main sequence at redshift z , and the values of the coefficients are $A = 0.21 \pm 0.10$, $B = -0.98 \pm 0.10$, $C = -0.49 \pm 0.03$, and $D = 0.03 \pm 0.04$ (where the quoted errors are 2σ uncertainties; Tacconi et al. 2020). The relation was obtained from a sample of 2052 galaxies with redshifts $z \approx 0\text{--}5.3$, stellar masses $M_{\star} \approx 10^9\text{--}10^{12.2} M_{\odot}$, and $\text{SFRs} \approx 0.04\text{--}5600 M_{\odot} \text{ yr}^{-1}$ (Tacconi et al. 2020).

We use Equation (1) to estimate the molecular gas depletion timescale of each of the 11,419 GMRT-CAT z 1 galaxies. Next, we combine the molecular depletion timescales of the individual galaxies with their SFRs to infer the molecular mass of each galaxy. Finally, we take a weighted mean of the M_{Mol} values in the two redshift subsamples, with the same weights (see Figure 1) that were used while stacking the HI 21 cm emission from each subsample. The estimated average molecular gas masses of the galaxies in the two redshift subsamples are listed in Table 1.

The errors on the coefficients A , B , C , and D were propagated via a Monte Carlo approach to estimate the formal error on the average molecular gas mass of each subsample, appropriately taking into account the weight associated with each galaxy in the subsample; these errors are listed in Table 1. Tacconi et al. (2020) note that systematic uncertainties in reduced quantities like the sSFR have little effect on the inferred $t_{\text{dep,mol}}$. This is even more the case for our sample of DEEP2 galaxies, which lie on the main sequence (C22a); we have further verified that even excluding the sSFR dependence

from Equation (1) has no significant effect on the average molecular gas mass. However, we note that the formal error on the average molecular gas mass for each subsample does not include uncertainties stemming from the assumptions (e.g., the CO-to- H_2 conversion factor, α_{CO}) made in the molecular gas mass estimates of the original sample of 2052 galaxies. Tacconi et al. (2020) estimate that the uncertainty arising from the assumptions is ≈ 0.25 dex; the effect of these uncertainties is discussed in Section 3.

Although Equation (1) was obtained from a sample of galaxies with $M_{\star} \approx 10^9\text{--}10^{12.2} M_{\odot}$ and at $z \approx 0\text{--}5.3$, the vast majority of M_{Mol} estimates in galaxies at $z \gtrsim 0.5$ are for objects with $M_{\star} \gtrsim 10^{10} M_{\odot}$ (e.g., Tacconi et al. 2020). The stellar mass of the DEEP2 galaxies in the GMRT-CAT z 1 survey extends down to $10^9 M_{\odot}$ at $z \approx 0.74\text{--}1.45$ (C22a), implying that we are applying the relation of Tacconi et al. (2020) in a regime where it is not well constrained. However, an alternative way to estimate the molecular gas masses of the DEEP2 galaxies is from the molecular gas depletion timescale, which is ≈ 0.7 Gyr in main-sequence galaxies at $z \approx 1$, with only a weak dependence on the stellar mass (Tacconi et al. 2013; Genzel et al. 2015). Assuming a constant molecular gas depletion timescale of 0.7 Gyr, we find that the inferred average M_{Mol} values for the GMRT-CAT z 1 galaxies are consistent with those obtained from Equation (1). It is hence unlikely that our estimates of the average M_{Mol} of star-forming galaxies at $z \approx 1.0$ and $z \approx 1.3$ are significantly affected by the above extrapolation to lower stellar masses.

2.4. Molecular Gas in Star-forming Galaxies at $z \approx 0$

We use the extended CO Legacy Database for GASS (Saintonge et al. 2017, xCOLD GASS) survey to compute the average molecular gas mass of a reference sample of blue star-forming galaxies at $z \approx 0$. The xCOLD GASS survey used the IRAM 30 m telescope to carry out CO(1–0) observations of a sample of 532 galaxies at $z \approx 0.01\text{--}0.05$ and with stellar masses $M_{\star} > 10^9 M_{\odot}$ (Saintonge et al. 2017). Approximately 90% of the xCOLD GASS galaxies are covered in the HI 21 cm line with the xGASS survey (Saintonge et al. 2017; Catinella et al. 2018), while stellar masses for all xCOLD GASS galaxies are again available from the MPA-JHU catalog. To carry out a fair comparison with our high- z blue star-forming galaxies, we restricted to the 287 blue xCOLD GASS galaxies, with $\text{NUV} - r < 4$; the stellar-mass distribution of the 287 galaxies is shown in Figure 1(A). A total of 252 of these galaxies have CO(1–0) detections, while 35 galaxies have upper limits on the CO(1–0) line luminosity (Saintonge et al. 2017). The xCOLD GASS catalog provides the molecular gas mass of the galaxies, including the mass contribution from helium. We computed the average molecular gas mass of these 287 galaxies, using weights in the average such that the stellar-mass distribution of the xCOLD GASS galaxies is identical to that in Figure 1(C), i.e., identical to that of the GMRT-CAT z 1 galaxies at $z = 1.25\text{--}1.45$. For the 35 galaxies with CO(1–0) nondetections, we assume that the molecular gas mass is equal to the 3σ upper limit on M_{Mol} , provided by the xCOLD GASS survey. The average molecular gas mass thus obtained is listed in Table 1; the error on this quantity was obtained from bootstrap resampling with replacement, accounting for the stellar-mass-based weight of each galaxy.

Table 2
The Ratios of the Average Masses of the Key Baryonic Constituents of Blue Star-forming Galaxies at $z \approx 0$, $z \approx 1$, and $z \approx 1.3$

| | $z \approx 0$ | $z \approx 1$ | $z \approx 1.3$ |
|---|---------------------------|------------------------|------------------------|
| Average atomic-gas-to-stars mass ratio, $\langle M_{\text{Atom}} \rangle / \langle M_{\star} \rangle$ | $0.54^{+0.17}_{-0.10}$ | $1.40^{+0.51}_{-0.35}$ | $4.44^{+1.65}_{-1.14}$ |
| Average molecular-gas-to-stars mass ratio, $\langle M_{\text{Mol}} \rangle / \langle M_{\star} \rangle$ | $0.095^{+0.029}_{-0.018}$ | $0.60^{+0.20}_{-0.13}$ | $0.89^{+0.30}_{-0.20}$ |
| Average atomic-gas-to-baryons mass ratio, $\langle M_{\text{Atom}} \rangle / \langle M_{\text{Baryon}} \rangle \times 10^2$ | $33.1^{+5.6}_{-4.2}$ | $46.6^{+5.8}_{-6.0}$ | $70.1^{+4.6}_{-5.4}$ |
| Average molecular-gas-to-baryons mass ratio, $\langle M_{\text{Mol}} \rangle / \langle M_{\text{Baryon}} \rangle \times 10^2$ | $5.78^{+1.01}_{-0.77}$ | $20.1^{+3.3}_{-2.9}$ | $14.1^{+2.8}_{-2.3}$ |
| Average stars-to-baryons mass ratio, $\langle M_{\star} \rangle / \langle M_{\text{Baryon}} \rangle \times 10^2$ | $61.1^{+6.5}_{-4.9}$ | $33.3^{+6.1}_{-5.8}$ | $15.8^{+3.6}_{-4.0}$ |
| Average atomic-to-molecular gas mass ratio, $\langle M_{\text{Atom}} \rangle / \langle M_{\text{Mol}} \rangle$ | $5.74^{+0.39}_{-0.37}$ | $2.32^{+0.54}_{-0.47}$ | $5.0^{+1.2}_{-1.0}$ |

Note. The first two rows list the ratios of the average atomic gas mass and the average molecular gas mass to the average stellar mass. The next three rows list the ratios of the average atomic gas mass, the average molecular gas mass, and the average stellar mass to the average total baryonic mass. Finally, the last row lists the ratio of the average atomic gas mass to the average molecular gas mass. The errors indicate the 1σ uncertainties in the estimates. See the text for discussion.

3. Results and Discussion

Table 1 lists our measurements of the average atomic gas mass, and estimates of the average molecular gas mass, of the GMRT-CATz1 galaxies at $z \approx 1.0$ and $z \approx 1.3$, along with measurements of the average atomic gas mass and average molecular gas mass of reference samples of blue star-forming galaxies at $z \approx 0$. The weights used in the averages ensure that the $z \approx 0$, $z \approx 1$, and $z \approx 1.3$ galaxy samples all have identical stellar-mass distributions, with an average stellar mass of $\langle M_{\star} \rangle = 10.3 \times 10^9 M_{\odot}$. We note that the listed errors on the $\langle M_{\text{Mol}} \rangle$ values do not include uncertainties in the assumptions (e.g., the value of α_{CO}). The uncertainty on $\langle M_{\star} \rangle$ is assumed to be 0.1 dex, based on comparisons between stellar-mass estimates for the same galaxies using different methods and assumptions (e.g., Stefanon et al. 2017). The last row of the table combines the estimates of the average atomic gas mass, average molecular gas mass, and the average stellar mass to estimate the average total baryonic mass of star-forming galaxies at $z \approx 0$, $z \approx 1.0$, and $z \approx 1.3$. The average baryonic mass, $\langle M_{\text{Baryon}} \rangle$, at each redshift interval was estimated using $\langle M_{\text{Baryon}} \rangle = \langle M_{\star} \rangle + \langle M_{\text{Atom}} \rangle + \langle M_{\text{Mol}} \rangle$.

Table 2 lists the ratios of the average atomic gas, molecular gas, and stellar masses relative to the average stellar mass and the average baryonic mass, as well as the ratio of the average atomic gas mass to the average molecular mass. We estimated the errors on each ratio via Monte Carlo simulations in which we obtained a large number of realizations of the ratio by drawing pairs of values for the average masses in the numerator and the denominator from Gaussian distributions of the two quantities, with the same means and standard derivations as the estimates of the average masses.

It is clear from Table 2 that the baryonic composition of star-forming galaxies shows dramatic evolution over the last ≈ 9 Gyr, from $z \approx 1.3$ to $z = 0$. Figure 3(A) plots the ratio of the average atomic gas and molecular gas masses (red squares and blue circles, respectively) to the average stellar mass versus redshift. The figure shows that both $\langle M_{\text{Mol}} \rangle / \langle M_{\star} \rangle$ and $\langle M_{\text{Atom}} \rangle / \langle M_{\star} \rangle$ decrease by roughly an order of magnitude from $z \approx 1.3$ to $z \approx 0$. However, the nature of the decline is very different in the atomic and molecular components. The ratio $\langle M_{\text{Atom}} \rangle / \langle M_{\star} \rangle$ drops steeply, by a factor of ≈ 3.2 , in the ≈ 1 Gyr period between $z \approx 1.3$ and $z \approx 1.0$, and then falls gradually, by a factor of ≈ 2.6 , over the ≈ 7 Gyr between $z \approx 1.0$ and $z \approx 0.0$. Conversely, the ratio $\langle M_{\text{Mol}} \rangle / \langle M_{\star} \rangle$ falls by a factor of only ≈ 1.5 between $z \approx 1.3$ and $z \approx 1.0$ but then drops by a factor of ≈ 6.3 between $z \approx 1$ and $z \approx 0$. The rapid

decline in the atomic gas mass of galaxies between $z \approx 1.3$ and $z \approx 1.0$, toward the end of the epoch of galaxy assembly, indicates insufficient accretion of gas from the CGM (C22a); this is the likely cause for the decline in the star formation activity of the universe at $z \lesssim 1$. Further, it is clear from Figure 3(A) that the atomic gas mass is significantly higher than the stellar mass, by a factor of ≈ 4.4 , at $z \approx 1.3$, during the epoch of peak star formation activity, $z \approx 1-3$, in the universe (Madau & Dickinson 2014).

Figure 3(B) plots the redshift evolution of the stellar, atomic gas, and molecular gas fractions of the baryonic mass. The three main baryonic components of galaxies show very different behaviors. In the local universe, it is clear that stars dominate the baryonic content of star-forming galaxies with $\langle M_{\star} \rangle \approx 10^{10} M_{\odot}$, constituting $\approx 60\%$ of the baryonic mass. However, the fraction of baryons in stars decreases with increasing redshift: Stars make up only 16% of the baryonic mass in such galaxies at $z \approx 1.3$. Conversely, Figure 3(B) shows that the contribution of both atomic gas and molecular gas to the total baryonic mass of star-forming galaxies with $\langle M_{\star} \rangle \approx 10^{10} M_{\odot}$ is significantly higher at $z \gtrsim 1$ than in the local universe. The contribution of atomic gas to the baryonic mass increases from $\approx 33\%$ at $z \approx 0$ to $\approx 47\%$ at $z \approx 1$, and then to $\approx 70\%$ at $z \approx 1.3$. For the molecular component, we find that $\langle M_{\text{Mol}} \rangle / \langle M_{\text{Baryon}} \rangle$ increases from $\approx 6\%$ at $z \approx 0$ to $\approx 20\%$ at $z \approx 1.0$ and then flattens, with $\langle M_{\text{Mol}} \rangle / \langle M_{\text{Baryon}} \rangle \approx 14\%$ at $z \approx 1.3$. Overall, Figure 3(B) shows that the neutral-gas fraction of the baryonic mass of star-forming galaxies with $\langle M_{\star} \rangle \approx 10^{10} M_{\odot}$ at $z \gtrsim 1$ is significantly higher than that at $z \approx 0$. Neutral gas makes up $\approx 84\%$ of the baryonic mass of star-forming galaxies at $z \approx 1.3$, with atomic gas constituting $\approx 70\%$ of the baryonic mass.

Finally, the values of the ratio of the average atomic gas mass to the average molecular gas mass in star-forming galaxies with $\langle M_{\star} \rangle \approx 10^{10} M_{\odot}$ at $z \approx 0$, $z \approx 1.0$, and $z \approx 1.3$ are listed in Table 1 and plotted against redshift in Figure 4. We find that $\langle M_{\text{Atom}} \rangle / \langle M_{\text{Mol}} \rangle$ decreases from $5.74^{+0.39}_{-0.37}$ in the local universe to $2.32^{+0.54}_{-0.47}$ at $z \approx 1$. Interestingly, however, we find that the ratio shows evidence for an increase at higher redshifts, $z > 1$, with $\langle M_{\text{Atom}} \rangle / \langle M_{\text{Mol}} \rangle = 5.0^{+1.2}_{-1.0}$ for galaxies with $\langle M_{\star} \rangle \approx 10^{10} M_{\odot}$ at $z \approx 1.3$. Atomic gas thus clearly dominates the cold gas content of star-forming galaxies at $z \approx 1.3$.

A possible source of error in our $\langle M_{\text{Mol}} \rangle$ estimates for the CATz1 galaxies lies in the extrapolation of Equation (1) to galaxies with stellar masses $\approx 10^9 M_{\odot}$ at $z \gtrsim 0.7$, a regime that is not tightly constrained by current data (Tacconi et al. 2020). However, the average $\langle M_{\text{Mol}} \rangle$ value is dominated by galaxies

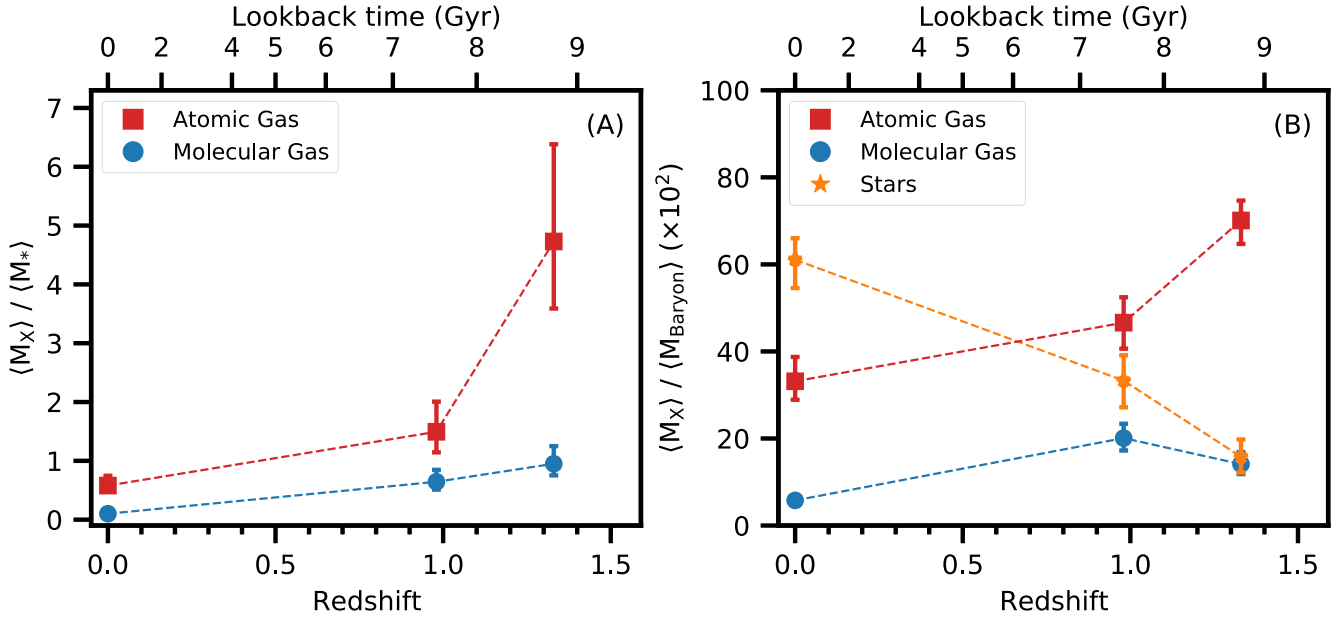


Figure 3. The redshift evolution of (A) the ratios of the average atomic gas mass and the average molecular gas mass to the average stellar mass, and (B) the ratios of the average atomic gas mass, the average molecular gas mass, and the average stellar mass to the average baryonic mass. In both panels, all plotted values are for stellar-mass-matched samples of galaxies with $\langle M_* \rangle \approx 10^{10} M_\odot$ at $z \approx 0$, $z \approx 1.0$, and $z \approx 1.3$. The error bars along the y-axis show the 1σ uncertainties in the estimates. See the text for discussion.

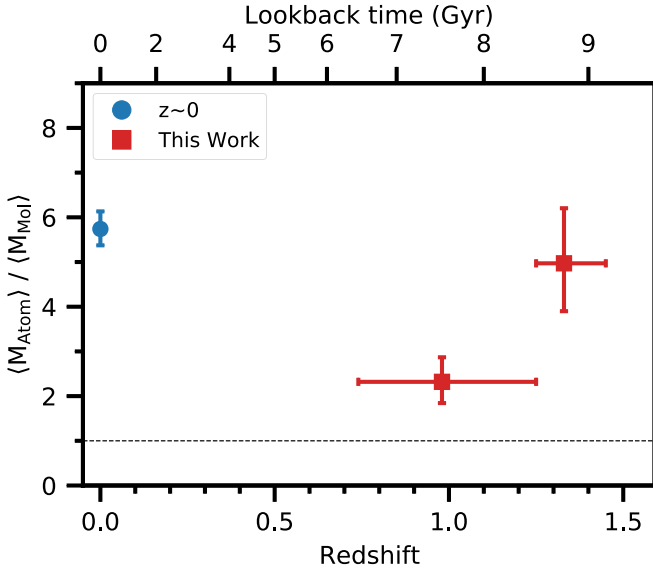


Figure 4. The ratio of the average atomic gas mass to the average molecular gas mass in stellar-mass-matched samples of star-forming galaxies at $z \approx 0$, $z \approx 1.0$, and $z \approx 1.3$. The blue circle shows the estimated value of $\langle M_{\text{Atom}} \rangle / \langle M_{\text{Mol}} \rangle$ in star-forming galaxies at $z \approx 0$ (Saintonge et al. 2017; Catinella et al. 2018). The red squares show estimates of $\langle M_{\text{Atom}} \rangle / \langle M_{\text{Mol}} \rangle$ in star-forming galaxies at two redshift intervals $z = 0.74\text{--}1.25$ and $z = 1.25\text{--}1.45$. The error bars along the y-axis show the 68.3% confidence intervals on $\langle M_{\text{Atom}} \rangle / \langle M_{\text{Mol}} \rangle$. The dashed line indicates $\langle M_{\text{Atom}} \rangle / \langle M_{\text{Mol}} \rangle = 1$. It is clear that the average atomic gas mass in star-forming galaxies is higher than the average molecular gas mass over the past 9 Gyr.

with $M_* > 10^{10} M_\odot$. Thus, even if we assume that the molecular gas masses of all galaxies with $M_* < 10^{10} M_\odot$ are systematically higher by a factor of ≈ 5 than the values obtained from Equation (1), this would only increase $\langle M_{\text{Mol}} \rangle$ at $z \approx 1.3$ by a factor of ≈ 2 , yielding $\langle M_{\text{Atom}} \rangle / \langle M_{\text{Mol}} \rangle \approx 2.5$ and $\langle M_{\text{Atom}} \rangle / \langle M_{\text{Baryon}} \rangle \approx 61\%$. Another possible source of error in the $\langle M_{\text{Mol}} \rangle$ estimates stems from the uncertainties in the assumptions (e.g., the value of α_{CO} , the dust-to-gas ratio, etc.)

made when originally determining the molecular gas masses that were used to obtain Equation (1); such uncertainties are expected to be $\approx \pm 0.25$ dex (Tacconi et al. 2020). However, even assuming that the “true” molecular gas masses are all 0.25 dex higher than those inferred from Equation (1), we find that our estimate of $\langle M_{\text{Atom}} \rangle / \langle M_{\text{Mol}} \rangle$ at $z \approx 1.3$ would decrease to 2.8 and of $\langle M_{\text{Atom}} \rangle / \langle M_{\text{Baryon}} \rangle$ to $\approx 63\%$. Thus, our conclusion that atomic gas dominates the cold gas content of star-forming galaxies at $z \approx 1.3$ appears to be robust against even relatively large uncertainties in the average molecular gas mass of high- z galaxies.

Figure 4 shows that atomic gas is the dominant component of the cold ISM of galaxies at both $z \approx 0$ and $z \gtrsim 1$. Spatially resolved HI 21 cm and CO studies in nearby galaxies find that H_2 arises in the inner, star-forming, regions of galaxies, while the HI is much more extended, extending to radii of tens of kiloparsecs (e.g., Leroy et al. 2008). Indeed, the molecular gas mass dominates the ISM in the central regions of spiral galaxies at $z \approx 0$, with the transition from a HI-dominated ISM to a H_2 -dominated ISM occurring at approximately half the optical radius, at a characteristic gas surface density of $\approx 14 M_\odot \text{pc}^{-2}$ (Leroy et al. 2008). For high- z galaxies, CO emission in star-forming galaxies has been found to have a half-light radius of $\lesssim 10$ kpc, similar to the size of the star-forming regions (e.g., Tacconi et al. 2013; Bolatto et al. 2015). Conversely, we find that the average HI 21 cm emission from star-forming galaxies at $z \approx 1$ is resolved for spatial resolutions < 90 kpc (C22b). It thus appears that the H_2 in high- z star-forming galaxies is also restricted to the central high-density regions while the HI extends out to tens of kiloparsecs in a significant fraction of such galaxies.

In this Letter, we have shown that the average atomic gas mass of star-forming galaxies with $\langle M_* \rangle \approx 10^{10} M_\odot$ is comparable to the average stellar mass at $z \approx 1$ and is significantly larger than both the average stellar mass and the average molecular gas mass at $z \approx 1.3$. We find that $\approx 70\%$ of the baryonic mass of star-forming galaxies with


$\langle M_{\star} \rangle \approx 10^{10} M_{\odot}$ at $z \approx 1.3$ is in atomic gas. Our results thus demonstrate that atomic gas dominates the baryonic content of star-forming galaxies at $z \approx 1.3$ during the epoch of peak star formation activity in the universe.

We thank the staff of the GMRT who have made these observations possible. The GMRT is run by the National Centre for Radio Astrophysics of the Tata Institute of Fundamental Research. We thank an anonymous referee for a very constructive report that helped increase the clarity of the paper. N.K. acknowledges support from the Department of Science and Technology via a Swarnajayanti Fellowship (DST/SJF/PSA-01/2012-13). A.C., N.K., and J.N.C. also acknowledge the Department of Atomic Energy for funding support, under project 12-R&D-TFR-5.02-0700.

Software: numpy (Harris et al. 2020), matplotlib (Hunter 2007).

ORCID iDs

Aditya Chowdhury  <https://orcid.org/0000-0002-5795-517X>

Nissim Kanekar  <https://orcid.org/0000-0002-9757-7206>

Jayaram N. Chengalur  <https://orcid.org/0000-0002-0269-1154>

References

Bera, A., Kanekar, N., Chengalur, J. N., & Bagla, J. S. 2019, *ApJ*, **882**, L7
 Bolatto, A. D., Warren, S. R., Leroy, A. K., et al. 2015, *ApJ*, **809**, 175
 Brinchmann, J., Charlot, S., White, S. D. M., et al. 2004, *MNRAS*, **351**, 1151
 Catinella, B., Saintonge, A., Janowiecki, S., et al. 2018, *MNRAS*, **476**, 875

Chowdhury, A., Kanekar, N., & Chengalur, J. N. 2022a, *ApJL*, **931**, L34
 Chowdhury, A., Kanekar, N., & Chengalur, J. N. 2022b, *ApJ*, in press
 arXiv:2207.00031
 Chowdhury, A., Kanekar, N., Chengalur, J. N., Sethi, S., & Dwarakanath, K. S. 2020, *Natur*, **586**, 369
 Chowdhury, A., Kanekar, N., Das, B., Dwarakanath, K. S., & Sethi, S. 2021, *ApJL*, **913**, L24
 Cortese, L., Catinella, B., & Janowiecki, S. 2017, *ApJL*, **848**, L7
 Cybulski, R., Yun, M. S., Erickson, N., et al. 2016, *MNRAS*, **459**, 3287
 Daddi, E., Bournaud, F., Walter, F., et al. 2010, *ApJ*, **713**, 686
 Davé, R., Anglés-Alcázar, D., Narayanan, D., et al. 2019, *MNRAS*, **486**, 2827
 Davé, R., Crain, R. A., Stevens, A. R. H., et al. 2020, *MNRAS*, **497**, 146
 Fernández, X., Gim, H. B., van Gorkom, J. H., et al. 2016, *ApJL*, **824**, L1
 Genzel, R., Tacconi, L. J., Lutz, D., et al. 2015, *ApJ*, **800**, 20
 Harris, C. R., Millman, K. J., van der Walt, S. J., et al. 2020, *Natur*, **585**, 357
 Hunter, J. D. 2007, *CSE*, **9**, 90
 Kauffmann, G., Heckman, T. M., White, S. D. M., et al. 2003, *MNRAS*, **341**, 33
 Lagos, C. D. P., Baugh, C. M., Lacey, C. G., et al. 2011, *MNRAS*, **418**, 1649
 Leroy, A. K., Walter, F., Brinks, E., et al. 2008, *AJ*, **136**, 2782
 Madau, P., & Dickinson, M. 2014, *ARA&A*, **52**, 415
 Mostek, N., Coil, A. L., Moustakas, J., Salim, S., & Weiner, B. J. 2012, *ApJ*, **746**, 124
 Newman, J. A., Cooper, M. C., Davis, M., et al. 2013, *ApJS*, **208**, 5
 Obreschkow, D., & Rawlings, S. 2009, *ApJL*, **696**, L129
 Popping, G., Somerville, R. S., & Trager, S. C. 2014, *MNRAS*, **442**, 2398
 Saintonge, A., Catinella, B., Tacconi, L. J., et al. 2017, *ApJS*, **233**, 22
 Salim, S., Dickinson, M., Michael Rich, R., et al. 2009, *ApJ*, **700**, 161
 Stefanon, M., Yan, H., Mobasher, B., et al. 2017, *ApJS*, **229**, 32
 Tacconi, L. J., Genzel, R., Saintonge, A., et al. 2018, *ApJ*, **853**, 179
 Tacconi, L. J., Genzel, R., & Sternberg, A. 2020, *ARA&A*, **58**, 157
 Tacconi, L. J., Neri, R., Genzel, R., et al. 2013, *ApJ*, **768**, 74
 Weiner, B. J., Coil, A. L., Prochaska, J. X., et al. 2009, *ApJ*, **692**, 187
 Whitaker, K. E., Franx, M., Leja, J., et al. 2014, *ApJ*, **795**, 104